Communication between the Active Sites in Dimeric Mercuric Ion Reductase: An Alternating Sites Hypothesis for Catalysis†

Susan M. Miller,*,‡ Vincent Massey,‡ Charles H. Williams, Jr.,‡,§ David P. Ballou,‡ and Christopher T. Walsh∥

Department of Biological Chemistry, University of Michigan Medical School, Ann Arbor, Michigan 48109, VA Medical Center, Ann Arbor, Michigan 48105, and Department of Biological Chemistry and Molecular Pharmacology, Harvard Medical School, Boston, Massachusetts 02115

Received August 31, 1990; Revised Manuscript Received December 12, 1990

ABSTRACT: Mercuric reductase, a flavoprotein disulfide oxidoreductase, catalyzes the two-electron reduction of Hg(II) to Hg(0) by NADPH. As with all the members of this class of proteins, the enzyme is a dimer of identical subunits with two active sites per dimer, each composed of one FAD and catalytically essential residues from both subunits. In the enzyme from Tn501, these residues include, at a minimum, FAD and cysteines 135 and 140 from one subunit and cysteines 558′ and 559′ from the other. With this sort of active site arrangement, the enzyme seems perfectly set up for some type of subunit communication. In this report, we present results from several titrations, as well as kinetics studies, that, taken together, are consistent with the occurrence of subunit communication. In particular, the results indicate that pyridine nucleotide complexed dimers of the enzyme are asymmetric. Since the EH_2–NADPH complex of the enzyme is the relevant reductant of Hg(II), these observations suggest that the enzyme may function asymmetrically during catalysis. An alternating sites model is proposed for the catalytic reduction of Hg(II), where both subunits of the dimer function in catalysis, but the steps are staggered and the subunits reverse roles after part of the reaction. An attractive feature of this proposal is that it provides a reasonable solution to the thermodynamic dilemma the enzyme faces in needing to both bind Hg(II) very tightly and reduce it.

Mercuric reductase is a flavoprotein that catalyzes the reduction of $Hg(SR)_2$ by NADPH as the final step in the detoxification of organomercurials and mercuric ion in a wide variety of bacterial strains (Foster, 1983; Summers, 1986; Silver & Misra, 1988). In its primary sequence and in its spectral properties mercuric reductase is strikingly similar to the pyridine nucleotide disulfide oxidoreductases, including glutathione reductase, lipoamide dehydrogenase, and trypanothione reductase (Fox & Walsh, 1982; Williams, 1991; Shames et al., 1986). These enzymes all contain both FAD and a redox-active disulfide at the active site (Williams, 1991), which is composed of $Cys_{135}Cys_{140}$ in Tn501-encoded mercuric reductase (Fox & Walsh, 1983; Brown et al., 1983). Unlike the other enzymes, however, mercuric reductase contains two additional thiol pairs, one in an 80-residue N-terminal extension ($Cys_{10}Cys_{13}$) and one near the C-terminus ($Cys_{558}Cys_{559}$ in Tn501-encoded enzyme) (Brown et al., 1983). The role of these three cysteine pairs has been examined by physical and chemical techniques with the wild-type enzyme and with a variety of site-directed mutants of the enzyme having one or more of these six cysteines changed to alanine or serine. These studies showed that the amino-proximal thiol pair ($Cys_{10}Cys_{13}$) is not essential for efficient reduction of Hg(II) (Fox & Walsh, 1983; Moore & Walsh, 1989). However, the carboxy-proximal thiol pair, $Cys_{558}Cys_{559}$, clearly communicates with the active-site dithiol pair, $Cys_{135}Cys_{140}$, and plays an essential role in binding and positioning Hg(II) for reduction (Miller, et al., 1989; Moore & Walsh, 1989). This carboxy-proximal cysteine pair, which is completely conserved in all sequences of mercuric reductases reported to date (Brown et al., 1983; Misra et al., 1985; Griffin et al., 1987; Wang et al., 1989) and which is absent from the other members of this class of flavoproteins, confers on mercuric reductase the unique ability to reduce the toxic Hg(II) ion rather than merely bind it.

Along with its homologous relatives, mercuric reductase is a dimer of identical subunits with one active site (FAD) per subunit. Crystal structure determinations of glutathione reductase (Thieme et al., 1981; Karplus & Schulz, 1987) and lipoamide dehydrogenase (Schierbeek et al., 1989) have shown that each active site in the dimeric enzymes is composed of residues from both subunits: FAD and redox-active disulfide from one subunit, and an essential histidine acid/base catalyst from the carboxy-terminal region of the other subunit. On the basis of this structure and the extensive similarities between mercuric reductase and glutathione reductase, Brown et al. (1983) speculated that the C-terminal cysteines of one monomer of mercuric reductase may be involved in Hg(II) binding at the FAD/dithiol site of the other monomer of the dimer. Distefano et al. (1990) have recently substantiated this hypothesis for the enzyme from Tn501 by generating active heterodimers from two inactive site-directed mutants, one lacking the active-site dithiol ($Ala_{135}Ala_{140}$), and the other lacking the carboxy-proximal dithiol ($Ala_{558}Ala_{559}$). Preliminary crystal structure data have further verified this hypothesis for mercuric reductase isolated from *Bacillus* sp strain RC607 (Schiering et al., 1990).

The requirement for this monomer–monomer interaction in normal activity raises the question of whether cooperative or half-sites behavior is present and, if so, whether it is important in the normal functioning of the enzyme. No clear evidence for such behavior has been reported for glutathione reductase. In lipoamide dehydrogenase, only two examples of nonidentical behavior have been reported. For wild-type enzyme, van Muiswinkel-Voetberg and Veeger (1973) reported

* To whom correspondence should be addressed.

† This work was supported by National Institutes of Health Grants GM 11106 (V.M.), GM 21444 (C.H.W.), GM 20877 (D.P.B.), and GM 21643 (C.T.W.).

‡ University of Michigan Medical School.
§ VA Medical Center.
∥ Harvard Medical School.

0006-2960/91/0430-2600$02.50/0

Scheme I: Redox States of Wild-Type Mercuric Reductase[a]

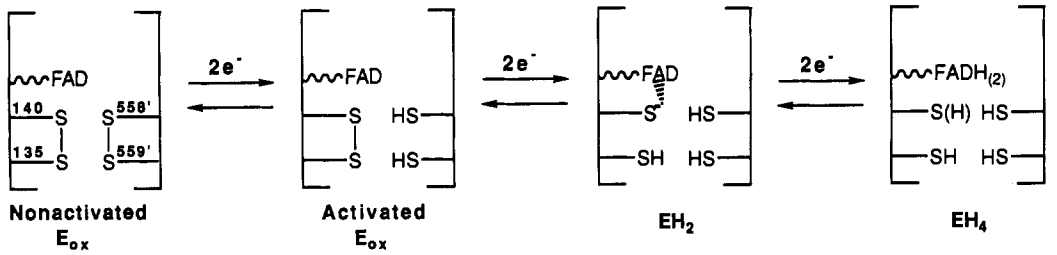

[a] The dashed-line symbol between FAD and S^- represents the charge-transfer interaction.

that binding of NAD^+ to the oxidized form of the enzyme occurs in a nonuniform manner, indicating the presence of two different NAD^+ binding sites. With lipoamide dehydrogenase that is monoalkylated on the interchange thiol, binding of NAD^+ gives rise to spectral changes indicative of the formation of a flavin C(4a)–thiol adduct; however, the changes indicate only 50% of the adduct is formed (Thorpe & Williams, 1981).

With mercuric reductase, two early observations with the wild-type enzyme suggested some type of site–site interaction: (1) Purified enzyme was found to bind ca. 0.7 equiv of $NADP^+$ per dimer after exhaustive dialysis against $NADP^+$-free buffer, suggesting the presence of one tighter and one weaker binding site per dimer (Fox & Walsh, 1982). (2) Reaction of the two-electron-reduced enzyme EH_2 with [^{14}C]iodoacetamide resulted in a biphasic loss of Hg(II) reductase activity concomitant with incorporation of radioactivity. However, spectral changes and the accompanying increase in transhydrogenation activity appeared to be complete in the fast phase of inactivation (Fox & Walsh, 1983). In the course of our studies on the properties of wild-type mercuric reductase and various Cys to Ala and Cys to Ser site-directed mutants, we have observed a variety of phenomena indicating nonequivalence in the properties of the subunits of the dimer. We present here examples of simple binding reactions, redox reactions, and kinetics studies of wild-type and mutant forms of the enzyme, all of which clearly exhibit differential behavior of the subunits. Based on these results, an alternating sites model for catalytic reduction of Hg(II) is developed, and the advantages of this type of model are discussed.

Experimental Procedures

Materials. Wild-type mercuric reductase was purified from *Escherichia coli* W3110 *lacI*^{q} containing the plasmid pPS01 [which contains the Tn501 mercuric reductase (*merA*) gene] as previously described (Miller et al., 1989). Specific Cys to Ala and Cys to Ser mutants of mercuric reductase were purified from the above strain of *E. coli* containing the modified plasmids as previously described (Moore & Walsh, 1989; Distefano et al., 1989; Miller et al., 1990; Schultz et al., 1985).

Methods. All experiments were conducted in 50 mM potassium phosphate buffer, pH 7.3, containing 0.3 mM EDTA (standard buffer), unless otherwise noted. UV–vis spectra were recorded with Cary 17 or 219 double-beam spectrophotometers or a Hewlett-Packard 8452A diode array spectrophotometer. Fluorescence spectra were recorded with a scanning ratio spectrofluorometer built by Gordon Ford and Dr. David Ballou at the University of Michigan. Rapid reaction studies were carried out with two different stopped-flow spectrophotometers with UV–vis absorbance capabilities: (1) One is equipped with a monochromator drive either for single-wavelength studies or for scanning spectra over a 7-s time scale (2-cm optical path) as previously described (Beaty & Ballou, 1981). (2) The other is equipped with a Tracor-Northern diode array detector for obtaining spectra of reaction intermediates on a millisecond time scale. Rapid reactions studied by fluorescence were carried out with a stopped-flow spectrofluorometer as previously described (Brissette et al., 1989). Anaerobic titrations were conducted in cuvettes with two side arms similar to those previously described (Williams et al., 1979). Samples were made anaerobic by subjecting the sample to several vacuum/nitrogen (or argon) equilibration cycles. Gases were made anaerobic by passing over a heated column of Ridox (Fisher).

Samples of wild-type EH_2 for titration with NADPH and $NADP^+$ were prepared by anaerobic reduction of E_{ox} with sodium dithionite. Titrations were made by using Hamilton gastight syringes equipped with threaded plungers.

Redox Titrations. Redox titrations were performed by using a new method (Massey, 1990). Xanthine oxidase (90 nM) and xanthine (670 μM) ($E_0' = -366$ mV; Green, 1934; Clark, 1960) were used as a source of electrons with a redox dye acting both as an electron mediator between the proteins and as a redox indicator. Methyl viologen ($E_0' = -449$ mV) was used for the Ser_{135} mutant mercuric reductase, and diquat ($E_0' = -361$ mV) was used for the Ser_{140} mutant. Experimentally, the enzyme of interest, an appropriate buffer, xanthine, and the indicator dye are placed in an anaerobic cuvette, with xanthine oxidase in a side arm. After anaerobiosis, xanthine oxidase is tipped in to start the reduction. The absorbance at both the λ_{max} of the enzyme and an appropriate wavelength for determining the amount of reduced indicator were then monitored.

Since the xanthine/xanthine oxidase method described here involves the continuous generation and equilibration of reducing equivalents, there is the possibility that incomplete equilibration would occur in the system whose potential is being measured. In order to avoid such complications, the concentration of xanthine oxidase added was adjusted such that reduction of the enzyme under study occurred over a period of 4–6 h, and halving the amount of xanthine oxidase added did not change the log/log plots used to determine redox potential. The enzyme potentials were calculated as derived in the Appendix.

Results

Since differential behavior has been observed in a number of different forms of both wild-type and mutant mercuric reductases, a description of the redox states of the enzyme, as well as the nomenclature of the mutant species, is presented here. Scheme I shows the several redox states of wild-type enzyme. Oxidized enzyme (E_{ox}) contains FAD and a redox-active disulfide ($Cys_{135}Cys_{140}$), as well as an auxiliary cysteine pair, $Cys_{558'}$ and $Cys_{559'}$ (primes indicate residues from the other subunit of the dimer). In enzyme fully activated toward Hg(II) reduction, the auxiliary pair exists as a dithiol, whereas in nonactivated enzyme (Sandstrom & Lindskog, 1987), it is a disulfide (Miller et al., 1989). E_{ox} forms of the enzyme do

not participate in turnover (Miller et al., 1986); rather, both disulfides must be fully reduced in a priming step to form active EH_2. In this form the Cys_{140} thiolate is highly stabilized ($pK_a \simeq 5.0$; unpublished results) and participates in a charge-transfer interaction with FAD, giving rise to the characteristic absorption spectrum of this species (e.g., Figure 2). Further addition of two electrons leads to formation of EH_4 with reduced flavin and all four thiols reduced.

Mutant mercuric reductases used in the present studies include those with mutations of either the N-terminal cysteines, the active-site disulfide, the C-terminal cysteines, or a combination of the active-site and C-terminal pairs. The di(Ala to Cys) mutant, $Ala_{10}Ala_{13}$, is a wild-type mimic, as was expected from previous proteolysis studies (Fox & Walsh, 1983). For mutations of the enzyme in the active-site and/or the C-terminal cysteines, we use a nomenclature where the one-letter codes for the cysteines or their replacements are listed in the order in which they come in the amino acid sequence (135, 140, 558, 559) (Distefano et al., 1990). Thus, wild-type enzyme (or the $Ala_{10}Ala_{13}$) is referred to as CCCC enzyme. A mutant having only Cys_{135} changed to alanine is referred to as ACCC enzyme, etc. Mutants having either or both cysteines 135 and 140 replaced by serine or alanine retain only the flavin as a redox center; they can only exist in two redox states, E-FAD and E-$FADH_{(2)}$. These mutants can be grouped into two types: those retaining Cys_{140}, which are EH_2 mimics since they still have the thiolate/flavin charge-transfer interaction that is present in wild-type EH_2, and those that have either serine or alanine at residue 140, which are E_{ox} mimics because they lack the charge-transfer interaction.

Evidence for Differential Behavior in Ligand Binding Processes

Spectral Changes upon Titration with NADP$^+$ of the E_{ox} Forms of Wild-Type and Several Mutant Mercuric Reductases. Mutations of the various cysteines in mercuric reductase generate minimal effects on the ability of the enzymes to bind pyridine nucleotides (Schultz et al., 1985; Distefano et al., 1989; Moore & Walsh, 1989). Hence, the E_{ox} form of all mercuric reductases binds NADP$^+$ to form an enzyme–product complex. The stoichiometry of binding has been determined to be 1 equiv of NADP$^+$ per FAD for the $Ala_{10}Ala_{13}$ enzyme at pH 7.3. Thus, when 50.2 μM NADP$^+$ was added to 17.2 μM enzyme monomer (final concentrations), and the enzyme was concentrated over a Centricon-30 membrane, 34 μM NADP$^+$ was found in the filtrate, giving, by difference, 16.2 μM bound NADP$^+$ or 0.94 equiv per FAD.

In spite of the simple stoichiometry of binding, the accompanying spectral changes are unusual. As illustrated in Figure 1A for the $Ala_{10}Ala_{13}$ enzyme at pH 7.3, binding of NADP$^+$ causes a dramatic change from the resolved UV–visible absorption spectrum of E_{ox} to one with little or no resolution in the 400–550-nm region. In contrast, the fluorescence excitation spectrum, Figure 1B, merely decreases in intensity, to a final value of 41–42% of the initial value, while maintaining the initial resolved form of pure E_{ox}. The same behavior has also been observed for this mutant at pH 5.1, and for wild-type enzyme and the CCCA, CCAC, CCAA (Moore, 1989), AACC, and CACC (Distefano 1989) mutant enzymes at pH 7.3. In each case the final absorbance spectrum loses resolution while the final fluorescence excitation spectrum does not change in shape but is reduced in intensity to between 40 and 45% of the starting value.

Fluorescence excitation spectra generally mimic the absorption spectrum of the fluorescent species. Hence, the above results are quite unexpected and suggest that NADP$^+$-bound

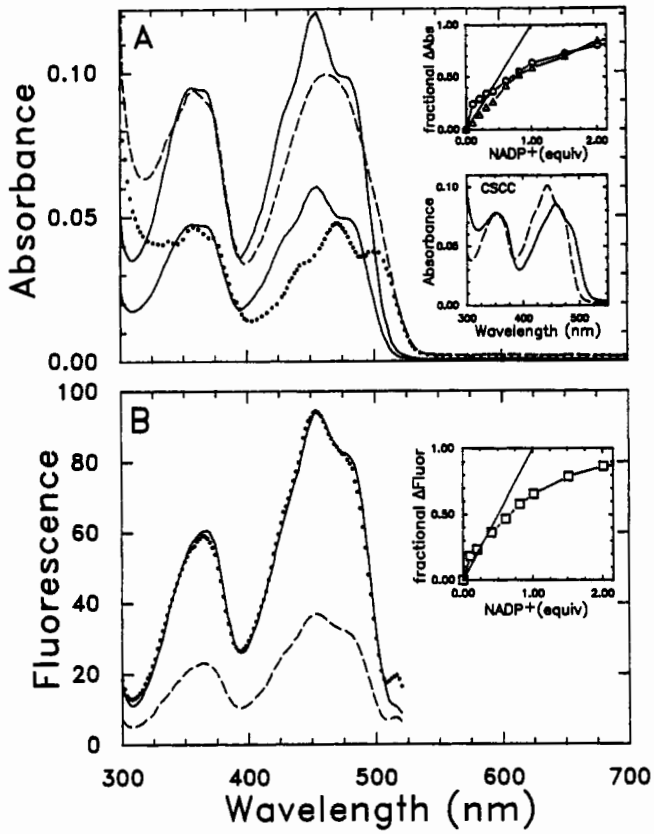

FIGURE 1: Binding of NADP$^+$ to the E_{ox} form of the $Ala_{10}Ala_{13}$ mutant mercuric reductase at pH 7.3. The $Ala_{10}Ala_{13}$ enzyme (10.6 μM) in standard buffer was titrated with NADP$^+$ and both the UV–visible absorbance spectra and the fluorescence excitation spectra (emission λ_{max} = 520 nm) were recorded at 4 °C. The sample was filtered before titration and after each addition through the same Gelman Acrodisc LC13 filter (0.45 μm). Panel A: Absorbance spectra shown are (upper solid) starting enzyme, (---) end point in the presence of 107.1 μM NADP$^+$, (lower solid) 0.5× starting enzyme, and (···) end point minus 0.5× starting enzyme. Upper inset shows the fractional change in absorbance at 456 nm (○) and 516 nm (△) vs equivalents of NADP$^+$ added per FAD as well as a line of unit slope. Lower inset shows E_{ox} form of the CSCC enzyme (8.3 μM) in the presence of (---) 0 NADP$^+$ and (—) 90.2 μM NADP$^+$. Panel B: Fluorescence excitation spectra (λ_{em} 525 nm) of (—) starting enzyme, (---) end point in the presence of 107.1 μM NADP$^+$, and (···) end point normalized to the initial intensity at 456 nm. Inset shows the fractional change in fluorescence intensity with excitation at 456 nm (□) vs the equivalents of NADP$^+$ added per FAD as well as a line of unit slope.

enzyme is a composite of two species, one with a dramatically altered UV–visible spectrum and totally quenched FAD fluorescence and one with essentially no change in the UV–visible spectrum and only a slight quenching of the fluorescence. Assuming that the final fluorescence excitation spectrum is the same as that of the UV–visible absorbance spectrum for one site of the enzyme, we can estimate the UV–visible spectrum of the altered site by subtraction from the final unresolved spectrum of the NADP$^+$-saturated species. Figure 1A also shows the spectrum of 50% of the unliganded enzyme and the result of subtracting this from the spectrum of E_{ox}–NADP$^+$. The difference spectrum (dotted line) suggests that the altered site has a spectrum similar in shape to uncomplexed enzyme but shifted ca. 15 nm to longer wavelength.

Corroboration of the above analysis comes from the binding of NADP$^+$ to the one anomalous mutant in this reaction, the CSCC enzyme. In this case, complexed enzyme exhibits a spectrum nearly identical in shape with that of the unliganded enzyme but shifted to longer wavelength by 16 nm and lowered in extinction (lower inset, Figure 1A). The nature of these

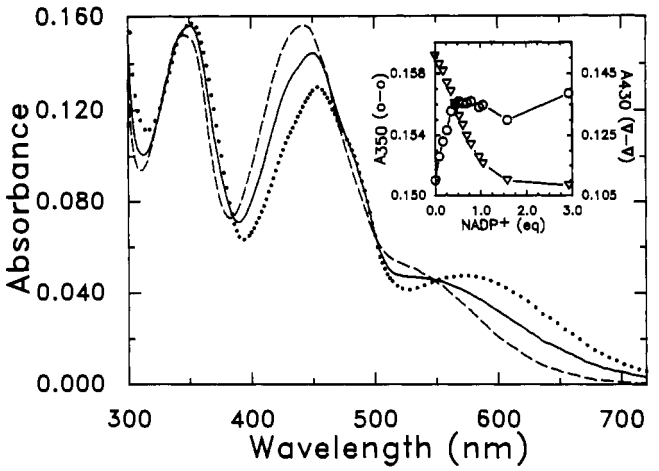

FIGURE 2: Titration of the EH_2 form of wild-type mercuric reductase with $NADP^+$ at 4 °C. Wild-type enzyme (17.4 μM) in standard buffer was titrated anaerobically to the EH_2 form with dithionite. After switching syringes, the EH_2 form of the enzyme was titrated with an anaerobic solution of $NADP^+$ and the absorbance spectra were recorded. Selected spectra are shown for (---) starting EH_2 enzyme, (—) after addition of 0.527 equiv of $NADP^+$ per FAD, and (···) end point after addition of 2.93 equiv of $NADP^+$ per FAD. Inset: absorbance at 350 nm (○) and at 430 nm (∇) as a function of the equivalents of $NADP^+$ added per FAD.

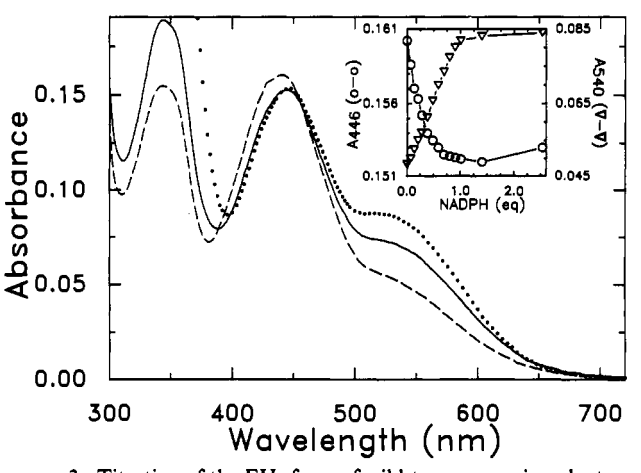

FIGURE 3: Titration of the EH_2 form of wild-type mercuric reductase with NADPH at 4 °C. Wild-type enzyme (17.7 μM) in standard buffer was titrated anaerobically to the EH_2 form with dithionite. After switching syringes, the EH_2 form was titrated with NADPH and the absorbance spectra were recorded. Selected spectra are shown for (---) starting EH_2 enzyme, (—) after addition of 0.587 equiv of NADPH per FAD, and (···) end point after addition of 2.52 equiv of NADPH per FAD. Inset: absorbance at 446 nm (○) and 540 nm (∇) as a function of the equivalents of NADPH added per FAD.

changes is consistent with those described above for the other enzymes, but here the changes appear to apply to both subunits. In contrast, the fluorescence excitation spectrum of the CSCC mutant shifts similarly to mimic that of the visible spectrum, but again the final intensity is only 40–50% that of the unliganded enzyme (each at their maximal λ_{ex}).

The finding that, in most of the mercuric reductase enzymes, the E_{ox}–$NADP^+$ complex is a composite of two species with different spectral properties indicates the presence of two conformationally different sites in the bound molecule. In addition, in the early part of the titration profiles for the binding of $NADP^+$ (insets, Figure 1), the fractional decreases in absorbance at 456 nm and fluorescence intensity are greater than the number of equivalents of $NADP^+$ added per FAD, but the total changes do not saturate until more than 1 equiv per monomer is added. At the same time, the changes at 510 nm appear to behave monophasically. These results suggest the presence of an intermediate in the binding process and possibly different affinities for the two sites. While the CSCC mutant shows spectrally identical species in the final complex, the titration profiles are distinctly biphasic (data not shown), again suggesting different affinities in that mutant. The different sites could be present on individual asymmetric dimers or could represent two populations of symmetric dimers. In either case, however, the results clearly indicate that there is some type of communication between the two halves of the dimeric enzyme molecule.

Titrations of Wild-Type EH_2 with $NADP^+$ and NADPH at pH 7.3. Since it is postulated that catalysis involves cycling between EH_2–NADPH and EH_2–$NADP^+$ (Miller et al., 1986, 1989), we have attempted to determine the binding constants for NADPH and $NADP^+$ to EH_2 by titration. The titrations are nearly stoichiometric, indicating that the dissociation constants are too low to measure accurately by spectral titration. Once again, however, nonidentical spectral changes occur in the two halves of the titration. Figures 2 and 3 display the results of titrations of EH_2 with $NADP^+$ and with NADPH, respectively. In each case the dashed line spectrum is that of unliganded EH_2, the solid line spectrum is the end point of the first half of the titration at ca. 0.5 equiv of pyridine nucleotide per FAD, and the dotted line is the final spectrum obtained in the presence of excess ligand. Different isosbestics appear in the first half of each titration than appear in the second half. In the first half of the titration with $NADP^+$ (Figure 2), clear isosbestics appear at 385, 453, 501, and 548 nm, and the absorbance at 350 nm increases. In the second half, the only simple isosbestic point shifts to 552 nm, while the region from ca. 475 to 500 nm becomes an isosbestic line and the absorbance of the 340–360-nm region does not change. Likewise, in the first half of the titration with NADPH (Figure 3), two clear isosbestics are found at 389 and 461 nm. In the second half, the region from 396 to 450 nm is essentially an isosbestic line. The clear delineation in the behavior of the two halves of the titrations suggests that the binding constant for the first site in each case is much tighter than for binding to the second site. However, even for the second site in each case the binding is too tight to determine accurately from these results. The most important conclusion from these data is that the EH_2 form of the enzyme also exhibits differential binding properties, again suggesting the presence of two conformationally different binding sites.

Titration of an EH_2 Mimic with NADPH. A beautiful example of distinctive behavior in the spectral changes of the two sites is provided by the titration of the ACCC mutant enzyme with NADPH at pH 8.5, Figure 4. This mutant retains its thiolate at Cys_{140} (pK_a = 6.2) and hence, spectrally mimics EH_2 with the thiolate/flavin charge-transfer band (dashed line in Figure 4). As shown in the inset to Figure 4, titration with NADPH gives an increase in the absorbance at 650 nm concomitant with a decrease in the absorbance at 440 nm during the first half of the titration, which is nearly stoichiometric with 0.5 equiv per FAD. In the second half of the titration, the absorbance changes at these two wavelengths are reversed, and the results indicate a weaker binding constant. The strikingly different changes in the wavelength range ca. 470–600 nm in the two halves of the titration should also be noted. These results clearly indicate the presence of an intermediate species in the binding process, resulting from some type of communication between the monomers of the dimeric enzyme molecule.

Formation of 50% of a Flavin C(4a)–S–Cys_{140} Adduct upon Binding of AADP[1] to the ACAA Mutant at pH 4.9. The

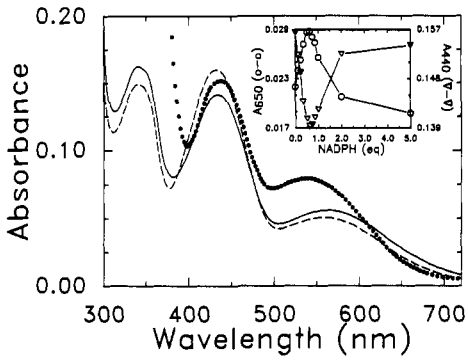

FIGURE 4: Titration of the ACCC mutant mercuric reductase with NADPH at pH 8.5 and 5 °C. The ACCC enzyme (18.6 μM) in 100 mM sodium pyrophosphate buffer, pH 8.5 (adjusted with acetic acid), containing 0.3 mM EDTA was titrated anaerobically with NADPH, and the absorbance spectra were recorded. Selected spectra are shown for (---) starting enzyme, (—) after addition of 0.501 equiv of NADPH per FAD, and (···) end point in presence of 5.03 equiv of NADPH per FAD. Inset: absorbance at 650 nm (O) and at 440 nm (▽) as a function of equivalents of NADPH added per FAD.

ACAA mutant mercuric reductase retains only one of the four active-site cysteines, Cys_{140} (the charge-transfer thiolate). At pH 4.9, where Cys_{140} is in the thiol form in this mutant (pK_a = 6.7), binding of $NADP^+$ leads to essentially complete formation of a flavin C(4a)–S–Cys_{140} adduct (Miller et al., 1990). The spectrum of this adduct consists of a single unresolved peak with λ_{max} = 382 nm and ϵ_{382} = 7.5 mM^{-1} cm^{-1}. In contrast, when the enzyme is titrated at pH 4.9 with the nonreducible $NADP^+$ analogue, 3-aminopyridine adenine dinucleotide phosphate (AADP) (Anderson et al., 1975), the behavior is clearly that of a half-sites reaction. As shown in Figure 5A, this nucleotide binds tightly to the enzyme, with spectral changes being complete upon the addition of an amount of AADP approximately equal to that of the enzyme flavin. However, instead of complete formation of the flavin C(4a) adduct (as observed with $NADP^+$), only approximately 50% of the enzyme flavin undergoes the conversion. This is illustrated in Figure 5B, where 50% of the initial spectrum is subtracted from that for the enzyme in the presence of excess AADP. The resulting difference spectrum, with a λ_{max} of 385 nm and a shoulder at ca. 320 nm, is very similar to the spectrum produced by $NADP^+$ (Miller et al., 1990), and has a comparable ϵ_{385} of 7.1 mM^{-1} cm^{-1} estimated by assuming 50% of the flavin has formed the adduct. The fluorescence of the enzyme-bound flavin was also followed during the course of the titration of Figure 5A (data not shown). The spectral shape of the excitation spectrum remained unchanged (excitation maxima at 360 and 446 nm), but with a saturating concentration of AADP the fluorescence intensity dropped to 11% of its initial value. From both the absorbance and fluorescence changes, an apparent K_d of 0.2 μM for AADP was calculated. It should be emphasized that the titration data show that while only one subunit forms the flavin C(4a) adduct, both subunits bind AADP tightly; this is demonstrated by the 89% decrease in the fluorescence intensity, and the plot (inset of Figure 5A) indicating tight binding. Here it can be seen that the extrapolated end point of 9.0 μM AADP for flavin C(4a) adduct formation is equal to the total enzyme flavin concentration.

Evidence for Differential Behavior in Redox Properties

Reduction Potentials of Uncomplexed Enzyme. The reported redox titration for wild-type mercuric reductase (Fox & Walsh, 1983) shows normal Nernstian behavior for the E_{ox} to EH_2 reduction (disulfide/dithiol) but was not extended to characterize the EH_2 to EH_4 reduction [$FAD/FADH_{(2)}$]. Instead a value for the EH_2/EH_4 couple was *calculated* from the measured value for the E_{ox}/EH_2 couple and the extent of disproportionation of EH_2 to E_{ox} and EH_4. Examination of the $FAD/FADH_{(2)}$ couple has been reported for a number of mutants where flavin is the only remaining redox center. In all of these, the reduction behavior appears to be non-Nernstian, but complete analyses of the peculiarities of the data are not presented (Schultz et al., 1985; Distefano et al., 1989). We present here reductive titrations of the SCCC and CSCC mutant enzymes and demonstrate that the data are consistent with there being two distinct reduction potentials for the enzyme-bound flavin.

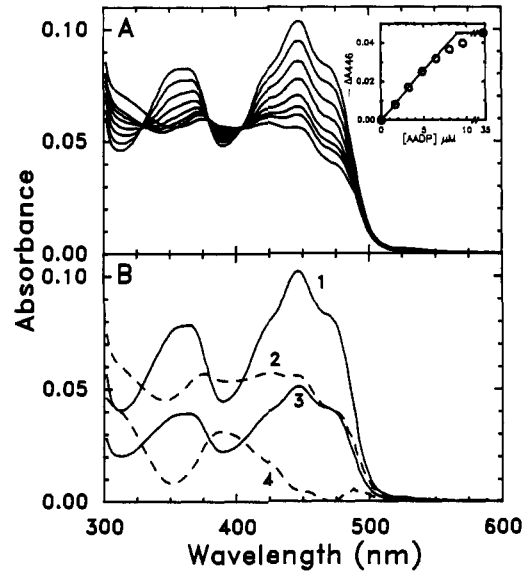

FIGURE 5: Effect of AADP on inducing only partial formation of the flavin C(4a)–cysteinyl adduct of mercuric reductase mutant ACAA. Panel A: The ACAA enzyme (9.0 μM) in 0.1 M acetate buffer, pH 4.9, at 4 °C was titrated with AADP, and spectra were recorded after each addition. Since AADP absorbs in the wavelength range below 380 nm, each spectrum was recorded vs a blank containing the same concentration of AADP. The curves with decreasing A_{446} were obtained before and after addition of 1.63, 3.25, 4.85, 6.44, 8.02, 9.59, and 33.4 μM AADP. There was no further change with a total of 54.6 μM AADP. The inset shows the decrease in A_{446} vs the concentration of AADP. Panel B: Spectral deconvolution of the effect of AADP. Curve 1, 9.0 μM ACAA mutant mercuric reductase in 0.1 M acetate buffer, pH 5.0. Curve 2, after addition of excess AADP (45 μM). Curve 3, curve 1 × 0.50. Curve 4, the result of the operation curve 2 − curve 3.

Figure 6 shows spectra obtained during a redox titration of the CSCC mutant at pH 7.68, using the xanthine/xanthine oxidase method of reduction with diquat as the indicator dye. For comparison, the inset shows the spectra of oxidized and reduced enzyme and oxidized and reduced diquat obtained separately. Figure 7A shows a Nernst plot of the titration, where log (ox/red) for the enzyme is calculated from the change in absorbance at 444 nm assuming only one species is present. [Note that log (ox/red) for the dye can be converted to E'_{obs} by substitution in the Nernst equation together with its midpoint potential (E'_0 = −361 mV; Fultz & Durst, 1982).] A similar Nernst plot is shown in Figure 7B for a titration of the SCCC mutant at pH 8.7 (data not shown), again using the xanthine/xanthine oxidase method with methyl viologen as the indicator dye. The dashed lines in Figure 7A,B are theoretical plots for a single redox center undergoing two-electron reduction vs an indicator dye undergoing one-

[1] Abbreviations: AADP, 3-aminopyridine adenine dinucleotide phosphate; $FADH_{(2)}$, reduced flavin of unknown protonation state.

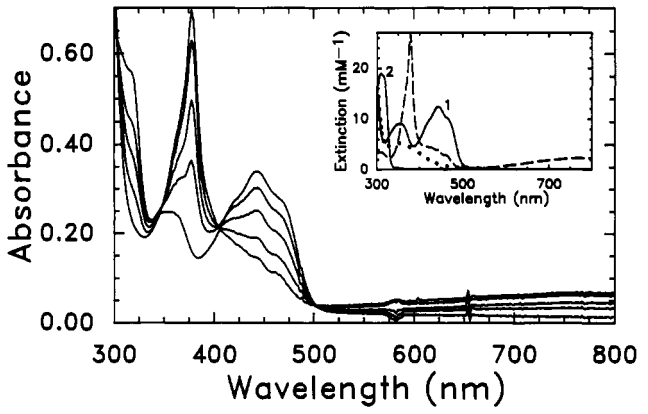

FIGURE 6: Redox titration of the CSCC mutant mercuric reductase at pH 7.68. The CSCC enzyme (27.5 μM) in 135 mM potassium phosphate buffer, pH 7.68, was mixed with 6 mM EDTA, 0.3 mM xanthine, 20 μM diquat, 2 μM methyl viologen, and 2 μM 5-deaza-5-carbaflavin (total volume = 1.004 mL) in an anaerobic cuvette. After anaerobiosis, 3.0 μL of a solution of xanthine oxidase (A_{450} = 0.3) was tipped in from the side arm and the absorption spectra were recorded over time for about 8 h with an HP 8425A diode array spectrophotometer. The end point of the titration was obtained by photoreduction after the xanthine/xanthine oxidase reaction had essentially stopped. Spectra shown with decreasing A_{444} were recorded at 0, 42, 105, and 275 min after tipping in the xanthine oxidase and, finally, at the end point after photoreduction. Inset shows the spectra of the oxidized (solid line 1) and reduced (···) enzyme and the oxidized (solid line 2) and reduced (- - -) diquat obtained independently.

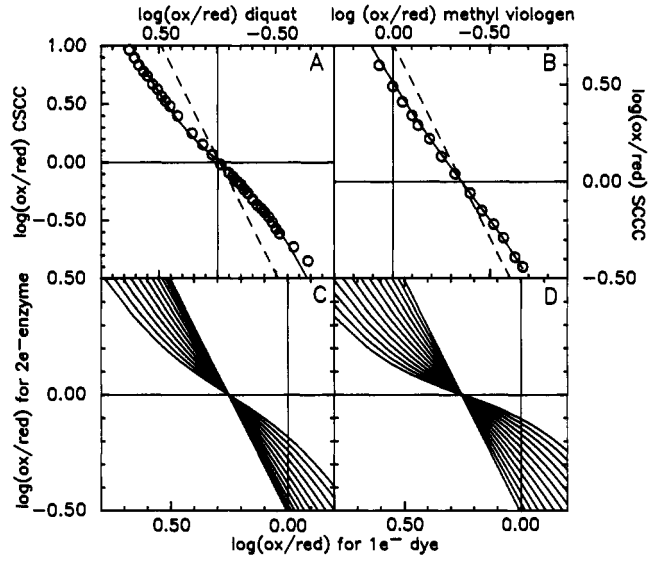

FIGURE 7: Nernst plots for the redox titrations of the CSCC and SCCC mutant mercuric reductases and the expected plots for the models of Scheme II. Panel A: Nernst plot for the titration of the CSCC enzyme shown in Figure 6. Log (ox/red) for the enzyme is calculated from the change in absorbance at 444 nm after correction for the contribution from reduced diquat. Log (ox/red) for diquat is calculated from the change in absorbance at 378 nm, which is an isosbestic point in the enzyme reduction. Circles are the data. The curve through the points is calculated as described in the text. The straight line is the theoretical Nernst plot expected for a single redox center. Panel B: Nernst plot for the titration of the SCCC enzyme at pH 8.7, using methyl viologen as the indicator dye. Log (ox/red) for the enzyme was calculated from the change in absorbance at 450 nm, and log (ox/red) for methyl viologen was calculated from the change in absorbance at 600 nm. Presentation as in panel A. Panel C: Expected behavior in a Nernst plot for a system with two independent but indistinguishable sites (Scheme IIA), where the difference between the two potentials has been varied from 0 (linear plot) to 60 mV (greatest curvature) in 5-mV increments. Panel D: Expected behavior in a Nernst plot for a symmetric dimer that exhibits negative cooperativity (Scheme IIB), where the difference between the first and second potentials was again varied from 0 (linear plot) to 60 mV (greatest curvature) in 5-mV increments.

Scheme II: Two-Site Models. (A) Asymmetric Dimer Model. (B) Negative Cooperativity Model in Which the Asymmetric Fully Bound Species Are Indistinguishable

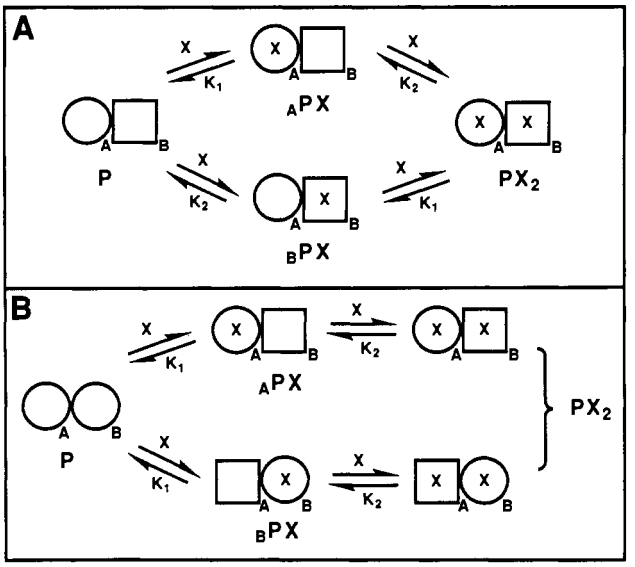

electron reduction; the lines are linear with a slope of 2 (Minnaert, 1965). However, the data plotted in Figure 7A,B are nonlinear and have slopes significantly less than 2.0 for the major portions that pass through the apparent midpoints [log (ox/red) for enzyme = 0]. These data clearly show more complex redox behavior than expected for a single redox center and indicate that the extent of reduction calculated from the spectral changes is actually a composite of the extent of reduction at more than one site, assuming the sites are spectrally indistinguishable.

In order to analyze these data, we have evaluated the expected behavior for log [ox_{total}/red_{total}] as a function of E'_{obs} for several model systems, and have found that the data can be adequately modeled by either of the two simplest but indistinguishable models for biphasic behavior of this type. Scheme IIA depicts an asymmetric dimer model where the two monomers of the homodimer, in spite of being identical in primary sequence, exhibit intrinsically different ligand binding affinities and reduction potentials, which do not change as a function of the occupancy or redox state of the other monomer. Scheme IIB depicts a negative cooperativity model (Koshland et al., 1966), where the dimer is initially symmetric in its properties but undergoes a transition upon binding or reduction of the first site to yield an intermediate asymmetric dimer with a lower binding affinity or more negative reduction potential (more difficult to reduce) for the "empty" monomer.

Derivation of the equations describing the behavior of these two models follows simple ligand binding theory and is shown in the Appendix. As illustrated by Figure 7C,D, either model gives nonlinear plots for log [ox_{total}/red_{total}] vs E'_{obs} with increasing curvature developing as the difference between the two potentials increases. In each case, the curve through the apparent midpoint is nearly linear and the slope decreases as the separation in the two potentials increases. As shown in the Appendix, measurement of this slope at the apparent midpoint of the titration provides a method for determining the separation between the apparent midpoint and the true potentials and, hence, the actual values for the potentials that will best fit the data for each of the models. The major difference between the two models in Scheme II is that the curvature increases and the slope decreases more quickly for the cooperative model than for the initial asymmetric model as $E'_1 - E'_2$ increases. However, an identical curve can be

Table I: Reduction Potentials Calculated from Two-Site Models[a]

calcd potentials	CSCC (pH 7.68) negative cooperativity	CSCC (pH 7.68) independent sites	SCCC (pH 8.7) negative cooperativity	SCCC (pH 8.7) independent sites
E_1'	−359	−351	−461	−453
E_2'	−389	−397	−479	−487
$E_1' - E_2'$	30	46	18	34

[a] See Appendix for calculations. All potentials are given in millivolts.

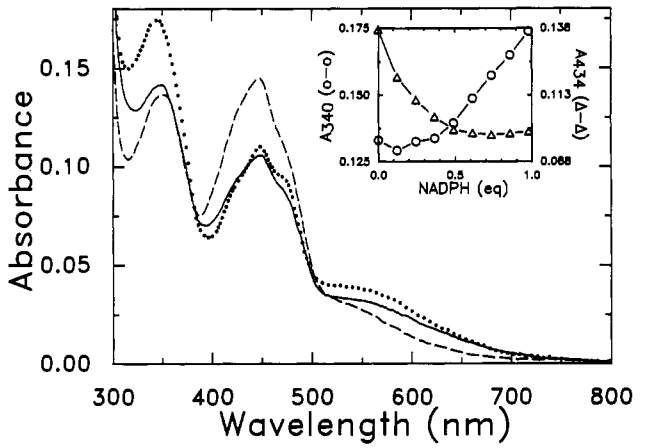

FIGURE 8: Titration of the EH_2 form of the $Ala_{10}Ala_{13}$ mutant mercuric reductase with NADPH at pH 5.1 and 4 °C. The $Ala_{10}Ala_{13}$ enzyme (17.0 μM) in 75 mM sodium acetate buffer, pH 5.1, containing 0.3 mM EDTA was titrated anaerobically to EH_2 with dithionite. The EH_2 form was then titrated anaerobically with NADPH and the spectra were recorded. Selected spectra are shown for (---) starting EH_2, (—) after addition of 0.5 equiv of NADPH per FAD, and (···) after addition of 1.0 equiv of NADPH per FAD. Inset: absorbance at 340 nm (○) and at 434 nm (△) as a function of the equivalents of NADPH added per FAD.

calculated from each model by using different values for E_1' and E_2'. The solid lines in Figure 7A,B are the theoretical curves calculated by using either model. Table I summarizes the values of the potentials calculated for both enzymes by using the two models. The fit of these two-potential models to the data for the SCCC mutant enzyme is excellent. It is also quite good for the CSCC mutant enzyme, considering that significant deviations from the fit only occur at either very low or very high fractional reduction, where the absorbance changes that provide the measure of reduction are more difficult to measure. While these data do not provide a means of distinguishing between the two models, they clearly indicate that the flavin, and, hence the active site, in mercuric reductase can exist in two different environments.

Reaction of the EH_2 Form of the $Ala_{10}Ala_{13}$ Mutant Enzyme with NADPH at pH 5.1. The observation of two distinct reduction potentials for enzyme-bound FAD in unliganded mercuric reductase leads us to question whether this is also seen in the catalytically relevant enzyme complex EH_2–NADPH. At pH 7.3, binding of NADPH to EH_2 is very tight but biphasic (Figure 3), indicating two different binding affinities and the possibility of different reduction potentials in the complex. At that pH, however, wild-type EH_2 is fully deprotonated ($pK_a \simeq 5.0$), and reduction of FAD by NADPH does not occur as a consequence of the strong donation of negative charge into the flavin ring by the adjacent Cys_{140} thiolate. However, at lower pH, where Cys_{140} is protonated, the reduction potential of the FAD should become more positive relative to NADPH, allowing reduction of flavin. Indeed, Sahlman et al. (1986) have shown that reduction of wild-type E_{ox} with excess NADPH at pH 5.1 yields a final

Scheme III: Redox and Protonation States of $Ala_{10}Ala_{13}$ Mutant at pH 5.1[a]

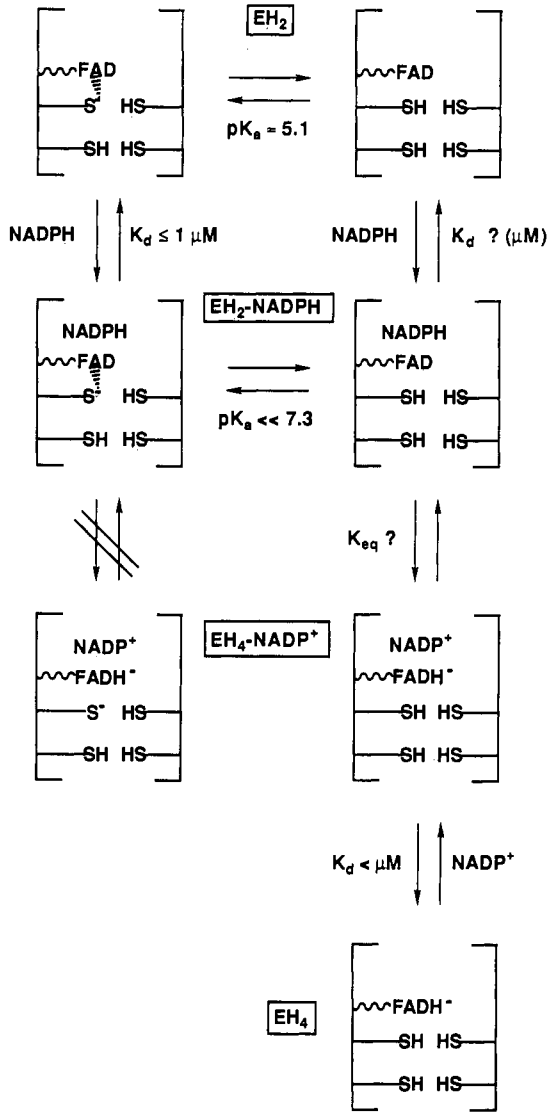

[a] The dashed-line symbol between FAD and S^- represents the charge-transfer interaction.

spectrum that appears to be largely reduced.

To determine whether reduction of FAD by NADPH is biphasic, we have titrated the EH_2 form of the $Ala_{10}Ala_{13}$ enzyme with NADPH at pH 5.1. Since this is near the thiol pK_a (5.0) of unliganded enzyme, the progress of the reductive titration will reflect the relative affinities of both protonated and unprotonated EH_2 and EH_4 species for NADPH and $NADP^+$, respectively, as well as the redox couple of complexed enzyme. Scheme III shows the relevant binding and redox equilibria for protonated and unprotonated noninteracting species. In spite of these complexities, reduction of a mixture of noninteracting species should proceed as a smooth redox titration as long as the protonation equilibria are rapid. Distinctly biphasic behavior would not be expected unless the protonation equilibrium of the complexed species is very slow.

Figure 8 shows that reduction of enzyme-bound flavin at pH 5.1 is *distinctly biphasic* Upon addition of the first 0.5 equiv of NADPH per FAD, a significant loss of absorbance in the 450-nm region occurs concomitant with an increase in absorbance at wavelengths between ca. 520 and 720 nm, consistent with reduction of FAD. Also, there is essentially no increase in absorbance at 340 nm, suggesting very little

accumulation of NADPH in this part of the titration. Upon addition of the second 0.5 equiv of NADPH per FAD, however, no further reduction of the flavin is indicated. Rather, there is a distinct increase in the absorbance at 340 nm indicative of the accumulation of NADPH, concomitant with the development of increased resolution in the 450-nm region and an increase in absorbance at wavelengths between ca. 500 and 650 nm, a pattern distinctly different from the first half of the titration, suggesting only binding of NADPH. *The simple model of Scheme III, in which protonation equilibria are established quickly, cannot adequately explain these data.* Once again the observations clearly indicate more complex behavior involving conformational inequality of the two species binding pyridine nucleotide. In this case, the tighter binding species undergoes reduction while the weaker binding species does not.

Beyond the addition of 1 equiv of NADPH, further reduction of the flavin occurs, but complete reduction requires more than 10 equiv of NADPH per FAD. This reaction was examined kinetically by mixing 10.4 μM $Ala_{10}Ala_{13}$ EH_2 with 104 μM NADPH (final concentrations) in a stopped-flow spectrophotometer equipped with a diode array detector. The dead-time spectrum is similar in shape to that of the spectrum from the titration after addition of 1 equiv of NADPH, but the overall absorbance is higher. Reduction of flavin in the complex then proceeds biphasically with rate constants of ca. 1 s^{-1} and 0.05 s^{-1}, stopping ca. 5–15% short of full reduction (data not shown). Thus, kinetically the two flavins also behave differently. Qualitatively, this behavior is similar to that observed in the reduction of the ACAA mutant with NADPH at pH 4.9. With that mutant, the flavin is totally reduced by excess NADPH in a biphasic manner with rate constants of ca. 260 s^{-1} and 32 s^{-1} (Miller et al., 1990).

Evidence for Differential Kinetic Behavior

Reaction of NADPH-Complexed AACC Mutant Mercuric Reductase with Oxygen. With both active-site cysteines mutated to alanines, the AACC mutant has no redox chemistry of the disulfide or charge-transfer interaction of thiolate with flavin. Hence, studies of this mutant may simplify characterization of the redox interactions of the flavin with NADPH, as well as the spectral properties of the FAD/NADPH and $FADH^-/NADP^+$ charge-transfer complexes. Upon addition of 1 equiv of NADPH per FAD to the E_{ox} form of the AACC enzyme, a mixture of 55–60% reduced flavin species and 40–45% oxidized species is produced. Addition of excess NADPH to the mixture does not alter this final level of reduction, but addition of 0.5 equiv of $NADP^+$ per FAD to the final mixture returns the level of reduction closer to a value of 50% (solid line, Figure 9). This 50% reduction is again very striking and suggests half-sites reactivity. However, it could simply reflect the poise of the bound flavin/pyridine nucleotide couples instead of two separate potentials. In contrast to the reduction of $Ala_{10}Ala_{13}$ enzyme (Figure 8), titration of the AACC mutant with NADPH is not distinctly biphasic. However, reoxidation of the complex with O_2 is biphasic.

In order to better characterize this process, we have examined the kinetics of reoxidation of the complexed AACC enzyme as a function of the oxygen concentration, using both absorbance and fluorescence stopped-flow spectroscopy. As shown in the kinetic traces (inset, Figure 9), the reoxidation of the complexed enzyme is distinctly biphasic. The observed rate constants for both phases show a hyperbolic dependence on oxygen concentration. This key observation indicates the formation of an enzyme–oxygen complex followed by the

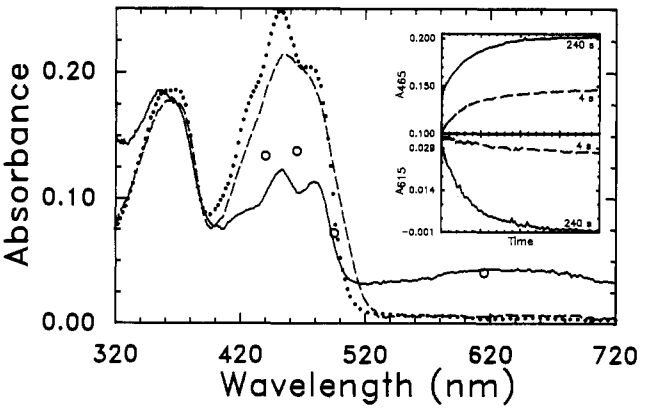

FIGURE 9: Stopped-flow reaction of the NADPH-complexed AACC mutant mercuric reductase with O_2. The AACC enzyme (21.7 μM) in standard buffer was titrated anaerobically with 1 equiv of NADPH. $NADP^+$ (0.5 equiv) was then tipped in from the side arm to give a final complex that appears to be 50% reduced in its 450-nm band. This complex was then mixed with equal volumes of the same buffer containing 2 mM, 0.5 mM, or 0.2 mM O_2 (before mixing) at 4 °C in a stopped-flow spectrophotometer capable of measuring both kinetics and spectra. (···) Spectrum of enzyme before titration recorded with a Hewlett-Packard diode array spectrophotometer; (—) spectrum of the initial complex before reaction and (- - -) spectrum of the final complex after reaction with O_2, both recorded with the stopped-flow spectrophotometer. The absorbance changes were monitored at 440, 465, 495, and 615 nm. Representative traces are shown in the insets for reaction with 1.0 mM O_2 (final concentration) monitored at 465 and 615 nm with time frames of (- - -) 4 s and (—) 240 s. The circles in the main graph show the end point of the fast phase calculated from the amplitudes of the absorbance changes at each wavelength occurring in the fast phase of the reaction.

Table II: Kinetic Constants for the Reaction of NADPH-Complexed AACC Mutant Mercuric Reductase with Oxygen

	by absorbance		by fluorescence	
phase	k_{ox} (s^{-1})	K_{O_2} (mM)	k_{ox} (s^{-1})	K_{O_2} (mM)
fast	2.45	0.6	3.10	0.8
slow	0.059	1.4	0.061	1.1

chemical conversion, in this case oxidation, according to (Strickland et al., 1975)

$$E_{red} + O_2 \underset{k_{off}}{\overset{k_{on}}{\rightleftharpoons}} E_{red}\text{–}O_2 \xrightarrow{k_{ox}} E_{ox} + H_2O_2 \qquad (1)$$

where $k_{obs} = (k_{ox}O_2)/(O_2 + K_{O_2})$ and $K_{O_2} = (k_{ox} + k_{off})/k_{on}$. The fact that *both phases* show this behavior further indicates that there must be two different types of reduced enzyme species that can bind and react with O_2. The kinetic constants, k_{ox} and K_{O_2}, obtained from double-reciprocal plots of $1/k_{obs}$ vs $1/O_2$ (y-intercept equals $1/k_{ox}$ and slope equals K_{O_2}/k_{ox}), are summarized in Table II and show very good correlation between the two spectroscopic methods. The rate constants for the reoxidation differ by 40–50-fold for the two phases; i.e., the two different reduced enzyme species react with O_2 at very different rates.

The observation of two saturable phases in the reaction could be consistent with either parallel reactions of noninteracting asymmetric subunits or with sequential reactions of cooperatively interacting subunits. Distinction between these two pathways lies in the characterization of the intermediate formed in the fast phase of the reaction. In either pathway, chemical intuition argues that O_2 would react more readily with the prereduced flavin site. Thus, with noninteracting subunits, the flavin should become fully oxidized in the fast phase of the reaction, while the slow phase should only involve oxidation of NADPH. With interacting subunits, the half-sites

Scheme IV: Model for Reaction of the NADPH-Complexed AACC Mutant with O_2

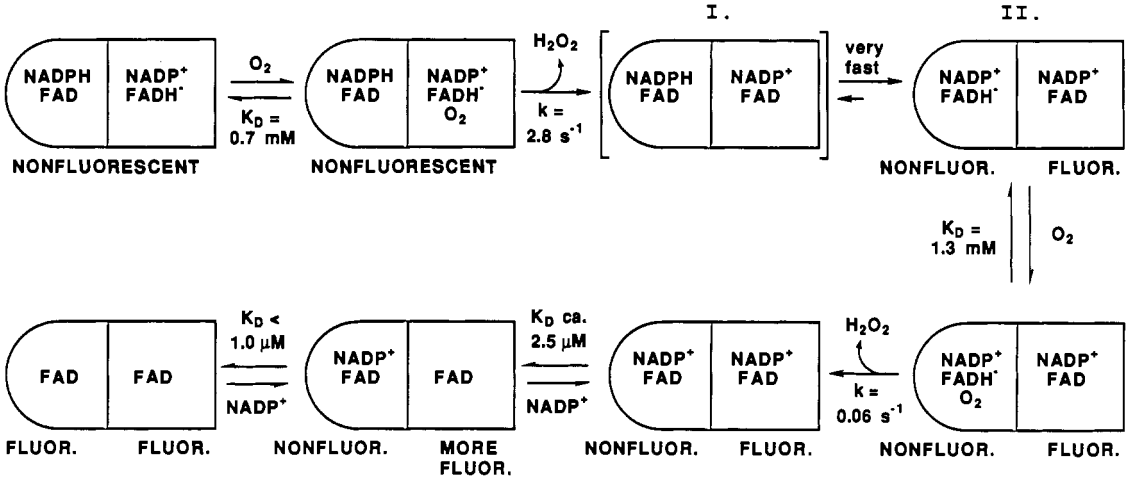

reduction observed in the starting complex could be alternately coupled, such that oxidation of the prereduced site would allow rapid reduction of the second site; thus, significant oxidation in the fast phase is not required.

Experimentally, the intermediate does indeed retain a significant amount of reduced flavin character. The circles in Figure 9 represent the absorbances at the end of the fast phase. Comparison of the circles to the starting spectrum of the partially reduced complexed enzyme (solid line) and to the final spectrum at the end of the slow phase (dashed line) (both taken in the stopped-flow spectrophotometer) shows that a large fraction of the flavin is still reduced at the end of the fast phase and at least 95% of the absorbance at 620 nm still remains.

Scheme IV shows the sequential cooperative model that accommodates these results. In this model, the initial complexed enzyme dimers are asymmetric with regard to their redox state, one monomer being reduced and bound to $NADP^+$ and the other being oxidized and bound to NADPH. Reaction of the reduced flavin site with O_2 yields a transient intermediate I, with both flavins oxidized, that rapidly undergoes electron transfer from NADPH to FAD on the second monomer, giving the observable intermediate II. This species should have a similar absorbance in the 600-nm region of the charge transfer band since that is where the $FADH^-/NADP^+$ charge transfer absorbance is maximal (Massey & Palmer, 1962; Blankenhorn, 1975). Additionally, the flavin region should still be at a similar level of reduction, but should have a somewhat different character since there is now an FAD/$NADP^+$ complex instead of the FAD/NADPH complex in the starting enzyme. Furthermore, this complex could be fluorescent since E_{ox}–$NADP^+$ complexes of these enzymes retain a significant amount of fluorescence (vide supra). Reaction of intermediate II in Scheme IV with O_2 will give the larger absorbance changes associated with formation of the fully oxidized dimer (---). At the end of the reaction, there is only 1.5 equiv of $NADP^+$ per FAD in the reaction mixture, which is not enough to fully saturate the enzyme. Thus, the return of fluorescence in the second phase may be due to dissociation of $NADP^+$, giving the more fluorescent unliganded species (vide supra).

The implications of the data are quite striking. It appears that binding of a ligand to one monomer of the dimeric enzyme can affect the reactivity of the other monomer by 40–50-fold. Stated another way, it says that the subunits of the dimeric enzyme molecule are not independent; rather, the reactivity of each subunit is strongly influenced by the ligands and redox state of the other subunit in the dimer.

Discussion

Numerous complexities in binding and kinetic properties of oligomeric proteins have been documented, and a variety of models have been proposed to explain them [for review, see Huang et al. (1982)]. As with unregulated monomeric enzymes, oligomeric enzymes having a uniform population of noninteracting subunits exhibit simple hyperbolic saturation curves in both steady-state kinetics and ligand binding. Deviations from this behavior indicate the occurrence of multiple binding and/or catalytic sites in the population of oligomer. Basically, three types of abnormal behavior have been observed: positive deviations from a hyperbolic curve, negative deviations, and half-sites reactivities. Positive deviations, i.e., sigmoidal increases in activity or extent of binding as a function of substrate or ligand concentration, are indicative of positive cooperativity, where during the course of binding or catalysis the enzyme is converted from a lower affinity state to a higher affinity state over a narrow range of ligand concentration. The most common models envision this occurring either in stepwise changes of the subunits on the oligomer (Koshland et al., 1966) or in a concerted transition between conformationally distinct but symmetrical oligomers with different affinities for ligand (Monod et al., 1965).

By contrast, negative deviations from simple hyperbolic curves (i.e., saturation requires a much higher concentration of ligand than expected) indicate that the higher affinity binding site is initially available in the unliganded oligomer rather than being unmasked during the binding process. This behavior can be described equally well by models invoking a sequential negative cooperative interaction between subunits (Koshland et al., 1966) or models invoking a preexisting asymmetry, which can include but do not require subunit interactions (see Scheme II). Additionally, enzyme heterogeneity can give rise to negative deviations and must be ruled out before making mechanistic conclusions. When negative deviations occur in steady-state turnover, the observation is usually that lower activity is associated with the higher affinity site, and higher activity requires saturation of a lower affinity site. Such behavior has been observed in the mitochondrial ATPase. Coupled with a variety of other experimental data, this observation led Choate et al. (1979) to postulate an alternating site cooperativity model for catalytic turnover in the ATPase. In this model, the oligomer functions asymmetrically so that binding reactions on one subunit are coupled to catalytic conversions on the other subunit, and after completion

of a full catalytic cycle, the subunits reverse roles. In this way, both subunits are catalytically functional but alternating in sequence.

Half-sites reactivity is essentially an extreme negative deviation, where the binding and steady-state kinetics may actually appear normal but the stoichiometry of the reaction is one-half of the available sites or even less in higher oligomers. Many examples of half-sites behavior have been described for the inactivation of enzymes by chemical modification (Rasool et al. 1976; Franzen et al. 1980; Stallcup & Koshland, 1973). While these observations provide clues to the possible existence of subunit interactions, the mechanistic significance is not always clear. More pertinent are observations of half-sites reactions involving catalytic substrates. Such examples include the binding of only 1 mol of tyrosine to the dimer of tyrosyl-tRNA synthetase (Bosshard et al., 1975) and the phosphorylation of histidine at only one of the two active sites of the $\alpha_2\beta_2$ heterotetrameric succinyl-CoA synthetase by ATP (Ramaley et al., 1967; Moffet et al., 1972). In the latter case, it was found that although only one catalytic site is initially phosphorylated in the absence of succinate, transfer of phosphate to succinate and completion of a catalytic cycle at that active site requires phosphorylation by ATP at the other site (Bild et al., 1980; Wolodko et al., 1981). Once again, as with the mitochondrial ATPase, it appears that an alternating sites cooperativity mechanism is at work in this enzyme, such that different parts of the catalytic mechanism occur simultaneously at the separate catalytic sites on the oligomer. The key point in this mechanism is that the half-sites or negative deviation behavior does not indicate a permanent asymmetry of the oligomer but rather a fluid functional asymmetry that occurs as a consequence of subunit communication (Bild et al., 1980).

With these ideas in mind, the questions to consider are what type of behavior is indicated by the observations collected here for mercuric reductase, and what hypotheses can be made about their mechanistic significance? Analysis of the data leads to a classification of the results into three somewhat overlapping categories of behavior, all carrying the common theme of a negative deviation from the simple behavior of a population of noninteracting enzyme species.

The first category of results includes titrations that exhibit distinctly biphasic spectral changes in which the first phase is nearly stoichiometric with the addition of 1 equiv of ligand per dimer and full saturation requires only 4–6 equiv of ligand per dimer. The tight stoichiometry of the first phase indicates that the dissociation constant for ligand from the tight-binding site is well below micromolar, while that for the weak-binding site (while still quite low) is at least 2 orders of magnitude larger. Experiments of this type include the titrations of wild-type EH_2 with $NADP^+$ and NADPH at pH 7.3 (Figures 2 and 3), the titration of the E_{ox} form of the ACCC mutant (an EH_2 mimic) at pH 8.5 (Figure 4), and the titration of the EH_2 form of the $Ala_{10}Ala_{13}$ enzyme with NADPH at pH 5.1 (Figure 8). The titrations of wild-type EH_2 and of the ACCC enzyme appear to be simple ligand binding processes; i.e., no reactions occur after binding. While these processes are clearly biphasic, the data are insufficient to state whether the fully bound complexes are symmetrical or asymmetrical. By contrast, in the titration of the $Ala_{10}Ala_{13}$ EH_2 enzyme with NADPH at pH 5.1, where redox chemistry occurs, asymmetry is evident both in the process and in the final complex, as only one flavin is reduced per dimer.

The characteristic of the second category of results is this distinct half-sites asymmetry of the fully liganded complex, exemplified by the last example above. The three other species exhibiting half-sites asymmetry include the E_{ox}–$NADP^+$ complexes of wild-type enzyme and a variety of mutants (Figure 1), as indicated by the discrepancy between the UV–visible and fluorescence excitation spectra of the fully bound species, the AADP complex of the ACAA enzyme at pH 5.0 (Figure 5), in which only 50% of the flavin C(4a)–thiol adduct forms, and the NADPH-complexed AACC enzyme (Figure 9), in which only one flavin per dimer is reduced. In contrast to the very biphasic titration profile for the $Ala_{10}Ala_{13}$ enzyme at pH 5.1, the profiles for the latter two examples appear to be monophasic, suggesting that the overall affinities for the two sites are similar in these examples even though different environments exist at each bound site. Different, but not widely disparate, affinities are indicated in the E_{ox}–$NADP^+$ titration, where the profile varies as a function of wavelength but does not show distinct breaks as in the examples of the first category.

The third category of equilibrium observations includes those where the titration process is not distinctly biphasic but analysis of the data shows the process to be complex. These include the E_{ox}–$NADP^+$ titrations, as already described, and the redox titrations of the various mutant enzymes. In this latter set of experiments (Figures 6 and 7), the spectral changes appear to be uniform throughout the titration and hence do not suggest the presence of any intermediates. However, the typical analysis of this kind of data clearly indicates that the absorbance changes as a function of the poised potential are inconsistent with reduction of a single two-electron acceptor. Adequate fits to the data are obtained with either negative cooperative or preexisting asymmetric two-site models, with differences between the two potentials depending on the model used. In any case, the potentials are not so far apart that the reductions become distinctly biphasic.

The overwhelming conclusion to be drawn from this collection of titrations is that the subunits of mercuric reductase behave asymmetrically. Whether the asymmetry is induced or preexists in the unliganded forms of the enzyme cannot be established from these data. However, that distinction is not fundamentally important since unliganded E_{ox} does not participate in catalysis (Miller et al., 1986) and unliganded EH_2 can only exist transiently under catalytic conditions due to the very tight binding of both oxidized and reduced pyridine nucleotides (this work; Sahlman et al., 1984). On the other hand, the observation of asymmetry in several liganded forms of the enzyme is much more interesting and raises the question of whether the asymmetry is catalytically relevant. None of the data presented here directly addresses the question of "cooperativity" in the normal catalytic reduction of Hg(II). However, the oxidation kinetics of the NADPH-complexed AACC enzyme by O_2 provide some provocative suggestions. These studies reveal a 40–50-fold difference in the oxygen reactivity of the sites in the dimeric complex, thereby confirming the asymmetric nature of the dimer and eliminating the possibility that the enzyme is simply present as a redox equilibrium mixture. Furthermore, analysis of the spectral changes is consistent with a subunit interaction in the reaction leading to the proposed alternating sites cooperativity model in Scheme IV, where reduction of the second subunit proceeds readily after oxidation of the first subunit, but oxidation of the reduced second subunit is inhibited due to the presence of $NADP^+$ rather than NADPH on the oxidized subunit.

The observation of kinetic inequivalence, consistent with a model requiring subunit interactions, is intriguing, particularly for an enzyme in which the active site is composed of residues

Scheme V: Proposed Alternating Sites Mechanism for Catalytic Reduction of Hg(II) by Wild-Type Mercuric Reductase[a]

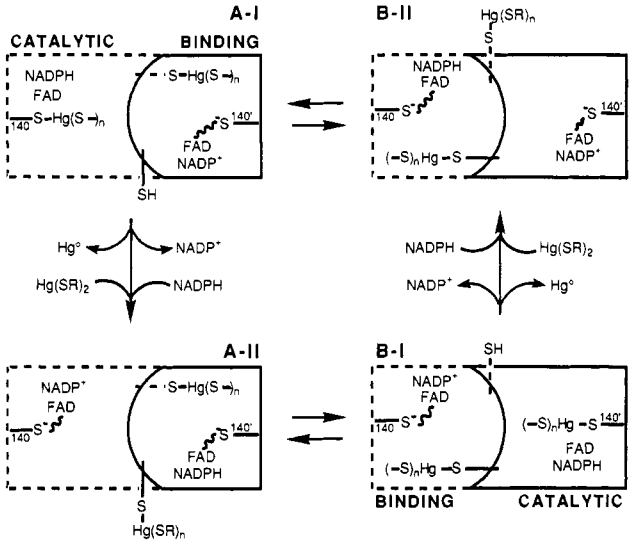

[a] In the Hg-thiol complexes, the subscript n may be 1 or 2; (-S) refers to enzyme thiols from Cys_{135} and Cys_{558} or Cys_{559}, with Cys_{558} being more likely on the basis of preliminary crystal structure data (Schiering et al., 1990); (SR) refers to small molecule thiols, which typically are 2-mercaptoethanol ligands in assays and may be glutathione ligands in vivo.

from both subunits of the dimer. Coupled with the multiple manifestations of thermodynamic inequivalence in both wild-type and mutant mercuric reductases, it strongly suggests a mechanistic role for subunit communication during the normal catalytic reaction of this enzyme. What functional advantage could be gained by inducing asymmetry in the dimer?

The major advantage may be that by functioning asymmetrically the enzyme can accomplish both of its thermodynamically conflicting roles of sequestering and reducing Hg(II) within the bacterial cell. To sequester the toxic metal ion, mercuric reductase must bind Hg(II) much more tightly than do other proteins. Since Hg(II) binds most tightly to thiols (basis of its toxicity), and since some proteins in the cell utilize dithiols for their activity, effective competition with those proteins may require a multithiol site with a suitable geometry for tight binding. For example, a three-coordinate trigonal planar complex should be at least 3 orders of magnitude more stable than a dithiol complex (Cheesman et al., 1988; Bowmaker et al., 1984). The dilemma, however, is that very tight binding by such a trithiol site (K_f may be 10^{45}–10^{50}; Casas & Jones, 1980; Cheesman et al., 1988) makes reduction a thermodynamically unfavorable reaction (E'_0 ca. -475 to -625 mV). This has been demonstrated for reduction of various Hg(II) complexes by reduced flavins in solution (Gopinath et al., 1989). Clearly, the enzyme must utilize some mechanism to bind Hg(II) tightly to sequester it, while also providing a weaker destabilized mode of binding to promote reduction.

In Scheme V, we present a hypothetical alternating sites mechanism for the catalytic reduction of Hg(II), in which tightly bound and weakly bound Hg(II) coexist on asymmetric dimers. In this model, catalysis occurs on both subunits of the asymmetric dimer, but the steps are staggered. The proposed catalytic subunit is fully primed with substrates and proceeds with transfer of electrons from NADPH to Hg(II) (e.g., A-I to A-II), while the proposed binding subunit sequesters Hg(II) and undergoes exchange of $NADP^+$ for NADPH in preparation for the next round of reduction. After these processes are complete, coupled conformational changes in the dimer invert the roles of the individual subunits (e.g., A-II to B-I), allowing completion of a full catalytic cycle on both subunits. Binding of substrates to the two types of sites is different but complementary. The catalytic subunit is proposed to bind NADPH tightly and utilize the energy derived from the tight binding to force Hg(II) into a less stable (weakly bound) complex, energetically more favorable for reduction. (For example, destabilization may result from a change in coordination geometry, perhaps trigonal planar to trigonal pyramidal, coupled with ligand exchange within the active site.) By contrast, the binding subunit is proposed to bind Hg(II) very tightly, satisfying the need to sequester Hg(II) from other proteins, but bind pyridine nucleotide weakly, thereby allowing the necessary exchange of $NADP^+$ for NADPH. Such an asymmetry in the binding of pyridine nucleotide to the dimer is strongly supported by the results presented above.

An important consequence of the staggered catalysis in an alternating sites mechanism is that steps that would be temporally separated during catalysis on a monomeric protein occur simultaneously at different sites on the asymmetric dimer. One obvious advantage of this in mercuric reductase is the simultaneous achievement of tight binding of one Hg(II) and reduction of another Hg(II). A more important advantage, however, is the coupling of energetically favorable reactions to energetically unfavorable ones to promote catalysis. As suggested above, tight binding of one substrate may be coupled to weak binding of the other substrate within each active site. However, the coupled conformational changes occurring across the dimer during the inversion of asymmetry may be fundamentally more important for catalysis. For example, in the case of the mitochondrial ATPase, it has been shown that, at low ATP concentrations, hydrolysis of ATP occurs on the enzyme at the high-affinity site, but product dissociation is extremely slow. When sufficient ATP is present to occupy the low-affinity site, the conformational readjustments of that subunit needed to make more favorable interactions with ATP are coupled to readjustments of the other subunit, resulting in a weakened binding of products and, hence, accelerated dissociation (Choate et al., 1979). The preferred binding of ATP versus products drives the conformational inversion needed for product dissociation and, hence, catalysis.

A similar situation may occur in mercuric reductase if, as proposed, the catalytic subunit binds pyridine nucleotides tightly but with a preference for NADPH. Tight binding of NADPH may facilitate reduction of Hg(II); however, tight binding of product $NADP^+$ is contradictory to efficient catalysis. As with the ATPase, a conformational change, converting a catalytic site into a binding site, could be essential to facilitate product dissociation. In the alternating sites model of Scheme V (as similarly proposed for the ATPase), this conformational conversion of a catalytic site (with $NADP^+$ bound) into a binding site (A-II to B-I) is coupled to the inverse conformational conversion of a binding site into a catalytic site. This conversion occurs as the protein readjusts to permit more favorable interactions with the substrate NADPH, which binds at least 10 times more tightly than $NADP^+$ to EH_2 (Sahlman et al., 1984). By coupling these reactions in time, i.e., making them concerted, energy released upon establishing favorable interactions with NADPH can be transferred directly, via the protein subunits, to weaken interactions with $NADP^+$, thereby lowering the activation energy for dissociation as needed for catalysis.

Appendix: Derivation of the Behavior of Log (ox_{total}/RED_{total}) vs E'_{obs} for a System with Two Spectrally Indistinguishable Redox Centers with Different Redox Potentials

An ideal redox titration of a single species follows the linear Nernst relationship:

$$E_{obs} = E'_m + 2.3RT/nF[\log (ox/red)] \quad (A1)$$

However, when two or more spectrally indistinguishable sites with different reduction potentials are present, the measurable quantity is

$$\log (ox_{total}/red_{total}) = \log [(ox_1 + ox_2 + ...)/(red_1 + red_2 + ...)] \quad (A2)$$

where the concentration of the oxidized (ox) and reduced (red) forms of each site depend on their respective midpoint potentials E'_1 and E'_2. Derivation of the relationship follows easily from treatment of the redox system as a ligand binding process. By use of the models in Scheme II, oxidized sites are equivalent to unliganded sites, reduced sites are equivalent to bound sites, and X is the electron, or electrons considered as a single ligand if the process appears to be concerted. In either model, P contains two oxidized sites, the intermediates, ${}_APX$ and ${}_BPX$, each contain one oxidized and one reduced site, and PX_2 contains two reduced sites. Thus

$$\frac{ox_{total}}{red_{total}} = \frac{2[P] + [{}_APX] + [{}_BPX]}{[{}_APX] + [{}_BPX] + 2[PX_2]} \quad (A3)$$

The concentrations of each species can be expressed in terms of the equilibrium dissociation constants K_1 and K_2 and will differ for the two models. For the asymmetric dimer model

$${}_APX = (P)(X)/K_1 \qquad {}_BPX = (P)(X)/K_2$$
$$PX_2 = (P)(X)^2/K_1K_2 \quad (A4)$$

which upon substitution into eq A3 and cancellation of P yields

$$\frac{ox_{total}}{red_{total}} = \frac{2 + X/K_1 + X/K_2}{X/K_1 + X/K_2 + 2(X^2/K_1K_2)} \quad (A5)$$

For the negative cooperativity model (Scheme IIB)

$${}_APX = {}_BPX = (P)(X)/K_1 \quad \text{and} \quad PX_2 = (P)(X)^2/K_1K_2 \quad (A6)$$

which yields

$$\frac{ox_{total}}{red_{total}} = \frac{2 + X/K_1 + X/K_1}{X/K_1 + X/K_1 + 2(X^2/K_1K_2)} = \frac{1 + X/K_1}{X/K_1 + X^2/K_1K_2} \quad (A7)$$

In either model, the subscripts 1 and 2 for the equilibrium constants reflect the different redox potentials for the sites. Thus

$$\frac{X}{K_1} = \frac{red_1}{ox_1} \quad \text{and} \quad \frac{X}{K_2} = \frac{red_2}{ox_2} \quad (A8)$$

regardless of which species are involved. The ratios of red/ox, in terms of reduction potentials are derived by rearrangement of the Nernst equations

$$E_{obs} = E'_1 + 2.3RT/nF[\log (ox_1/red_1)] \quad (A9)$$

$$E_{obs} = E'_2 + 2.3RT/nF[\log (ox_2/red_2)] \quad (A10)$$

to yield

$$red_1/ox_1 = 10^{0.034(\Delta E_1)} \quad (A11)$$

$$red_2/ox_2 = 10^{0.034(\Delta E_2)} \quad (A12)$$

where $nF/2.3RT = 0.034\ mV^{-1}$ when $n = 2$ electrons and $T = 298$ K, and $\Delta E_1 = E'_1 - E_{obs}$ and $\Delta E_2 = E'_2 - E_{obs}$, expressed in millivolts. Substitution of the relationships in eqs A11 and A12 into eqs A5 and A7 yields

$$\log \frac{ox_{total}}{red_{total}} = \log \frac{2 + 10^{0.034(\Delta E_1)} + 10^{0.034(\Delta E_2)}}{10^{0.034(\Delta E_1)} + 10^{0.034(\Delta E_2)} + 2[10^{0.034(E_1' + E_2' - 2E_{obs})}]} \quad (A13)$$

for the asymmetric dimer model and

$$\log \frac{ox_{total}}{red_{total}} = \log \frac{1 + 10^{0.034(\Delta E_1)}}{10^{0.034(\Delta E_1)} + 10^{0.034(E_1' + E_2' - 2E_{obs})}} \quad (A14)$$

for the negative cooperativity model.

From these expressions it is clear that plots of log (ox_{total}/red_{total}) vs E_{obs} will be nonlinear as illustrated in Figure 7C,D. However, as the slopes of the curves are nearly linear through the apparent midpoint, it is of value to determine the relationship of the slope at the midpoint to the difference in potential. The slope of each curve is found by taking the derivative as a function of E_{obs}. Thus, for the asymmetric dimer model

$$\text{slope} = \frac{d[\log (ox_{total}/red_{total})]}{d(E_{obs})} = \frac{0.068}{2 + 10^{0.034(\Delta E_1)} + 10^{0.034(\Delta E_2)}} + \frac{0.068[10^{0.034(E_1' + E_2' - 2E_{obs})}]}{2[10^{0.034(E_1' + E_2' - 2E_{obs})}] + 10^{0.034(\Delta E_1)} + 10^{0.034(\Delta E_2)}} \quad (A15)$$

At the apparent midpoint, E_{am}, $E'_1 + E'_2 - 2E_{obs} = 0$ and we define the absolute distance of the potentials from the apparent midpoint $\Delta E = E'_1 - E_{am} = -(E'_2 - E_{am})$. Thus, for the asymmetric dimer, eq A15 reduces to

$$\text{slope} = \frac{4(0.034)}{2 + 10^{0.034\Delta E} + 10^{-0.034\Delta E}} \quad (A16)$$

Rearrangement to

$$\Delta E = 29.6 \times \left(\log \left[\frac{-2 + 4(0.034)/\text{slope} + \{[2 - 4(0.034)/\text{slope}]^2 - 4\}^{1/2}}{2} \right] \right) \quad (A17)$$

allows calculation of the two potentials (in millivolts) for the asymmetric dimer model resulting in that slope.

Similar derivatization of eq A14 for the negative cooperativity model yields

$$\text{slope} = 0.034 \frac{1 + 2(10^{0.034\Delta E_2}) + 10^{0.034(E_1' + E_2' - 2E_{obs})}}{1 + 10^{0.034\Delta E_1} + 10^{0.034\Delta E_2} + 10^{0.034(E_1' + E_2' - 2E_{obs})}} \quad (A18)$$

which at the apparent midpoint reduces to

$$\text{slope} = 0.034 \left(\frac{2 + 2(10^{-0.034\Delta E})}{2 + 10^{0.034\Delta E} + 10^{-0.034\Delta E}} \right) \quad (A19)$$

Again, with slope = s, rearrangement to

$$\Delta E = 29.6 \times \left(\log \left[\frac{2 - 59.1s + \{[2(1 - 29.6s)]^2 - 4(29.6s)(29.6s - 2)\}^{1/2}}{59.1s} \right] \right) \quad \text{(A20)}$$

allows calculation of the potentials (in millivolts) for the negative cooperativity model consistent with the slope.

References

Anderson, B. M., Yuan, J. H., & Vercellotti, S. V. (1975) *Mol. Cell. Biochem. 8*, 89–96.

Beaty, N. B., & Ballou, D. P. (1981) *J. Biol. Chem. 256*, 4611.

Bild, G. S., Janson, C. A., & Boyer, P. D. (1980) *J. Biol. Chem. 255*, 8109–8115.

Blankenhorn, G. (1975) *Eur. J. Biochem. 50*, 351–356.

Bosshard, H. R., Koch, G. L. E., & Hartley, B. S. (1975) *Eur. J. Biochem. 53*, 493–498.

Bowmaker, G. A., Dance, I. G., Dobson, B. C., & Rogers, D. A. (1984) *Aust. J. Chem. 37*, 1607–1618.

Brissette, P., Ballou, D. P., & Massey, V. (1989) *Anal. Biochem. 181*, 234–238.

Brown, N. L., Ford, S. J., Pridmore, R. D., & Fritzinger, D. C. (1983) *Biochemistry 22*, 4089–4095.

Casas, J. S., & Jones, M. M. (1980) *J. Inorg. Nucl. Chem. 42*, 99–102.

Cheesman, B. V., Arnold, A. P., & Rabenstein, D. L. (1988) *J. Am. Chem. Soc. 110*, 6359–6364.

Choate, G., Hutton, R. L., & Boyer, P. D. (1979) *J. Biol. Chem. 254*, 286–290.

Clark, W. M. (1960) *Oxidation-Reduction Potentials of Organic Systems*, p 437, Williams & Wilkins Co., Baltimore, MD.

Distefano, M. D. (1989) Ph.D. Dissertation, Massachusetts Institute of Technology, Cambridge, MA.

Distefano, M. D., Au, K. G., & Walsh, C. T. (1989) *Biochemistry 28*, 1168–1183.

Distefano, M. D., Moore, M. J., & Walsh, C. T. (1990) *Biochemistry 29*, 2703–2713.

Foster, T. (1983) *Microbiol. Rev. 47*, 361–409.

Fox, B., & Walsh, C. T. (1982) *J. Biol. Chem. 257*, 2498–2503.

Fox, B. S., & Walsh, C. T. (1983) *Biochemistry 22*, 4082–4088.

Franzen, J. S., Ashcom, J., Marchetti, P., Cardamone, J. J., Jr., & Feingold, D. S. (1980) *Biochim. Biophys. Acta 614*, 242–255.

Fultz, M. L., & Durst, R. A. (1982) *Anal. Chim. Acta 140*, 1–18.

Gopinath, E., Kaaret, T. W., & Bruice, T. C. (1989) *Proc. Natl. Acad. Sci. U.S.A. 86*, 3041–3044.

Green, D. E. (1934) *Biochem. J. 28*, 1550.

Griffin, H., Foster, T., Silver, S., & Misra, T. (1987) *Proc. Natl. Acad. Sci. U.S.A. 84*, 3112.

Huang, C. Y., Rhee, S. G., & Chock, P. B. (1982) *Annu. Rev. Biochem. 51*, 935–971.

Karplus, P. A., & Schulz, G. E. (1987) *J. Mol. Biol. 95*, 701–729.

Koshland, D. E., Jr., Némethy, G., & Filmer, D. (1966) *Biochemistry 5*, 365–385.

Massey, V. (1990) in *Flavins and Flavoproteins, Tenth International Symposium Proceedings*, Walter de Gruyter, New York (in press).

Massey, V., & Palmer, G. (1962) *J. Biol. Chem. 237*, 2347–2358.

Miller, S. M., Ballou, D. P., Massey, V., Williams, C. H., Jr., & Walsh, C. T. (1986) *J. Biol. Chem. 261*, 2081–2084.

Miller, S. M., Moore, M. J., Massey, V., Williams, C. H., Jr., Distefano, M. D., Ballou, D. P., & Walsh, C. T. (1989) *Biochemistry 28*, 1194–1205.

Miller, S. M., Massey, V., Ballou, D., Williams, C. H., Jr., Distefano, M. D., Moore, M. J., & Walsh, C. T. (1990) *Biochemistry 29*, 2831–2841.

Minnaert, K. (1965) *Biochim. Biophys. Acta 110*, 42–56.

Misra, T. K., Brown, N. L., Haberstroh, L., Schmidt, A., Goddette, D., & Silver, S. (1985) *Gene 34*, 253–262.

Moffet, F. J., Wang, T., & Bridger, W. A. (1972) *J. Biol. Chem. 247*, 8139–8144.

Monod, J., Wyman, J., & Changeux, J.-P. (1965) *J. Mol. Biol. 12*, 88–118.

Moore, M. J. (1989) Ph.D. Dissertation, Massachusetts Institute of Technology, Cambridge, MA.

Moore, M. J., & Walsh, C. T. (1989) *Biochemistry 28*, 1183–1194.

Ramaley, R. F., Bridger, W. A., Moyer, R. W., & Boyer, P. D. (1967) *J. Biol. Chem. 242*, 4287–4298.

Rasool, C. G., Nicolaidis, S., & Akhtar, M. (1976) *Biochem. J. 157*, 675–686.

Sahlman, L., Lambeir, A.-M., Lindskog, S., & Dunford, H. B. (1984) *J. Biol. Chem. 259*, 12403–12408.

Sahlman, L., Lambeir, A., & Linkskog, S. (1986) *Eur. J. Biochem. 156*, 479–488.

Sandstrom, A., & Lindskog, S. (1987) *Eur. J. Biochem. 164*, 243–249.

Schierbeek, A. J., Swarte, M. B. A., Dijkstra, B. W., Vriend, G., Read, R. J., Hol, W. G. J., Drenth, J., & Betzel, C. (1989) *J. Mol. Biol. 206*, 365–379.

Schiering, N., Fritz-Wolf, K., Kabsch, W., Moore, M. J., Distefano, M. D., Walsh, C. T., & Pai, E. F. (1990) in *Flavins and Flavoproteins, Tenth International Symposium Proceedings*, Walter de Gruyter, New York (in press).

Schultz, P. G., Au, K. G., & Walsh, C. T. (1985) *Biochemistry 24*, 6840–6848.

Shames, S. L., Fairlamb, A. H., Cerami, A., & Walsh, C. T. (1986) *Biochemistry 25*, 3519–3526.

Silver, S., & Misra, T. K. (1988) *Annu. Rev. Microbiol. 42*, 717.

Stallcup, W. B., & Koshland, D. E. (1973) *J. Mol. Biol. 80*, 41–62.

Strickland, S., Palmer, G., & Massey, V. (1975) *J. Biol. Chem. 250*, 4048–4052.

Summers, A. O. (1986) *Annu. Rev. Microbiol. 40*, 607.

Thieme, R., Pai, E. F., Schirmer, R. H., & Schulz, G. E. (1981) *J. Mol. Biol. 152*, 763–782.

Thorpe, C., & Williams, C. H., Jr. (1981) *Biochemistry 20*, 1507–1513.

van Muiswinkel-Voetberg, H., & Veeger, C. (1973) *Eur. J. Biochem. 33*, 285–291.

Wang, Y., Moore, M., Levinson, H., Silver, S., Walsh, C., & Mahler, I. (1989) *J. Bacteriol. 171*, 83.

Williams, C. H., Jr. (1991) in *Chemistry and Biochemistry of Flavoenzymes* (Müller, F., Ed.) Vol. 3, CRC Press, Inc., Boca Raton, FL (in press).

Williams, C. H., Jr., Arscott, D. L., Matthews, R. G., Thorpe, C., & Wilkinson, K. D. (1979) *Methods Enzymol. 62D*, 185.

Wolodko, W. T., O'Connor, M. D., & Bridger, W. A. (1981) *Proc. Natl. Acad. Sci. U.S.A. 78*, 2140–2144.